

# Ab initio study of negative electron affinity on the scandium-terminated diamond (100) surface for electron emission devices

Ramiz Zulkharnay<sup>\*</sup>, Neil L. Allan, Paul W. May

School of Chemistry, University of Bristol, Cantock's Close, Bristol, BS8 1TS, United Kingdom

## ARTICLE INFO

### Keywords:

Diamond  
Density functional theory  
Negative electron affinity  
Surface  
Thermionic electron emission  
Scandium

## ABSTRACT

Surface modification of diamond with the addition of (sub)monolayer of metals or other electropositive adsorbates than the bulk carbon can result in negative electron affinity (NEA). Surface coverages of up to one-monolayer (<1 ML) of scandium on clean, oxygenated and nitrogenated diamond (100) surfaces were studied via plane-wave density functional theory (DFT) calculations. Adsorption of Sc on diamond is energetically favourable; for example, 0.25 ML coverage of Sc on the oxygenated diamond (100) surface has an extremely large calculated adsorption energy per adsorbate atom of  $-8.68$  eV. Moreover, the majority of stable Sc-adsorption configurations possess NEA, with the most negative values of  $-3.73$  eV,  $-3.02$  eV and  $-1.75$  eV being found for 0.25 ML Sc coverage on the oxygenated, bare and nitrogenated diamond surfaces, respectively. These results predict that Sc termination on diamond should provide a thermally stable surface with large NEA, and is therefore a highly promising candidate for thermionic and other electron-emission applications.

## 1. Introduction

Diamond has a unique combination of properties that distinguish it as an extraordinarily promising material for fundamental applications in scientific and technological advances [1]. The possibility of diamond being fabricated with a thermally stable surface exhibiting negative electron affinity (NEA) is currently of great interest for numerous electron-emission applications, such as photodetectors [2,3], field-effect transistors (FET) [4–6], and thermionic electron emitters [7,8]. Diamond with both an NEA surface and a low work function also has potential for applications such as photoelectrochemical CO<sub>2</sub> conversion [9], thermionic power generation and thermal-energy harvesting [8, 10].

NEA can be created by terminating the carbon bonds at the diamond surface with atoms or groups of atoms that are more electropositive than bulk carbon (Pauling electronegativity, EN = 2.55). This forms an electric dipole perpendicular to the surface with the positive charge outermost, lowering the barrier to emission of electrons which reside in the conduction band (CB). In the case of NEA (Fig. 1), the vacuum level lies below the CB minimum, such that there is now no barrier for emission of CB electrons [11–13]. For diamond, termination with atomic H produces NEA on the (100), (111) and (110) surfaces [11,13–16]. However, due to desorption of the H atoms at temperatures above

700 °C [10,17], hydrogenated diamond surfaces are unsuitable for high-temperature devices. Thus, there is a need to find alternative diamond surface terminations which possess a large NEA (*i.e.* more negative) while remaining stable at elevated temperatures.

Group I metals have long been known to exhibit NEA characteristics when adsorbed on diamond. However, the heavier metals, such as Cs, have low thermal stability which limits their usefulness at higher temperatures [12]. As such, computational and experimental work has focused upon elements that can provide a more thermally robust surface in addition to NEA, especially lighter Group I metals, such as Li [18,19], as well as various first-row transition metals (TMs), including Cu, Ni, Ti, V and Zn [20–23]. Results suggest that for metals deposited directly onto the diamond surface, carbide-forming metals give larger NEA values.

Although direct bonding of metal atoms to the diamond surface is a promising approach, many metallic elements do not readily form bonds with carbon. Even if a stable metal-carbon bond is possible, in many cases the deposited metal layer rapidly oxidises on exposure to air. One approach to overcome these problems is to deposit the metal onto an already oxidised diamond surface [24,25]. While it may appear counterintuitive to terminate the diamond surface with electronegative oxygen (EN = 3.44) in order to promote NEA, provided a sufficiently electropositive metal is bonded on top of the oxygen layer, the overall surface-charge distribution can produce a net NEA. An added benefit in

<sup>\*</sup> Corresponding author.

E-mail address: [ramiz.zulkharnay@bristol.ac.uk](mailto:ramiz.zulkharnay@bristol.ac.uk) (R. Zulkharnay).

<https://doi.org/10.1016/j.carbon.2022.04.067>

Received 22 February 2022; Received in revised form 22 April 2022; Accepted 23 April 2022

Available online 26 April 2022

0008-6223/Crown Copyright © 2022 Published by Elsevier Ltd. All rights reserved.

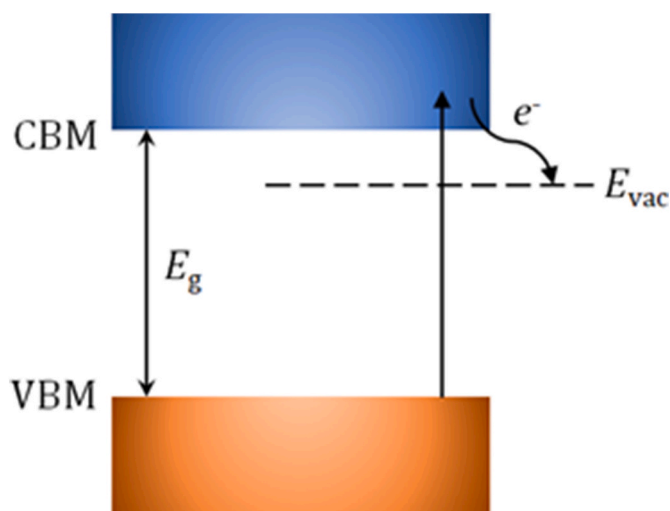


**Fig. 1.** Schematic energy diagram with relative positions of the conduction band minimum (CBM), valence band maximum (VBM) and vacuum energy level ( $E_{vac}$ ) for an NEA surface. High-energy electrons at the VBM are excited into the CB via external factors (e.g. thermal energy or photon absorption) and can then be subsequently emitted into the vacuum without having to overcome a barrier.  $E_g$  is the band gap, defined as the difference between the CBM and VBM.

these M–O–C systems is that the metal is already partially oxidised, lowering its reactivity towards further oxidation thereby making the surface more air stable.

An added complication in M–O–C systems is that oxygen can bond to the diamond (100) surface in a variety of configurations, including as a ketone (C=O), bridging ether (C–O–C), hydroxyl (OH) [26,27], or more complex multiatom structures [28]. The subsequent metal adsorbate can have very different mechanical and electronic properties depending upon the structure of this underlying oxide layer [29,30]. Various methods are used to oxidise diamond, including exposure to an oxygen plasma, or to a UV ozone lamp in air, or treatment with strong acids, but they all produce a mixture of ketone and ether configurations, and sometimes other structures, in varying proportions. Thus, the oxide layer, and hence the overlying metal layer, is often very inhomogeneous, with some parts of the surface experimentally exhibiting large NEA values while others show positive electron affinity (PEA) [31].

This mixture of oxygen surface configurations, where the ratio of ketone-to-ether is rarely known and difficult to control, has made studies of the M–O–C system challenging. Studies of these M–O–C terminated surfaces have again focused both experimentally and computationally on the use of Group I and II metals, such as Li and Mg [18,23–25,32,33], and TMs such as Cu, Ni, Ti, Zn [29] and Sn [34]. Other diamond-termination strategies using Si, Ge, B, metal nitrides, amines and OH groups have also been studied, with varying degrees of success, all of which are reviewed in Ref. [10]. These data sets suggest that for optimal NEA, together with an air- and temperature-stable diamond surface, it is preferable for the metal adsorbate to have the following attributes: (a) a high electropositivity, (b) a relatively small radius, (c) propensity to form highly charged positive ions, and (d) ready formation of bonds with both C and O. For example, Li and Mg are two of the most promising candidates so far tested, with the Mg–O–C system exhibiting the largest NEA to date, of  $-2.01 \pm 0.05$  eV [24,25].

With this in mind, we recently reported studies on two other likely candidates, Al and Ti, both of which fit the four criteria. Experimental measurements for Al termination ( $<1$  ML) on the clean and oxidised diamond (100) and (111) surfaces gave EA values of approximately  $-1.0$  eV, and work functions of  $\sim 4.5 \pm 0.5$  eV, depending upon the deposition method, coverage and annealing temperature [31]. These values were in broad agreement with those predicted by computer

simulations of Al + O (sub)monolayers on a diamond surface [35,36]. Similar NEA and work function values were reported from combined experimental and computational studies of Ti on bare and oxidised diamond, although these values were very dependent upon the Ti coverage, annealing conditions and oxygen geometry [37]. This study [37] was also the first to report metal adsorption studies on a nitrogenated diamond surface, *i.e.* Ti–N–C, and demonstrate that the M–N–C scenario is also a viable option for an NEA surface.

We now consider scandium as another likely NEA candidate due to its relatively small ionic radius ( $0.75 \text{ \AA}$ ), electropositive character (EN = 1.36) and propensity to form a highly charged cation ( $\text{Sc}^{3+}$ ). Moreover, Sc reacts readily with C, O and N, and is chemically similar to Al. To the best of our knowledge, Sc has not yet been studied in the context of NEA on diamond. Thus, the aim in this paper is to study theoretically, in detail, (sub)monolayer Sc adsorption onto clean, oxygenated and nitrogenated diamond, in order to identify a diamond surface with both large NEA and high thermal stability ( $>1200 \text{ }^\circ\text{C}$ ). Such a surface hopefully will afford a high electron-emission yield at low temperatures ( $\sim 500 \text{ }^\circ\text{C}$ ), will not degrade during use, and be compatible with commercial thermionic energy converters (TECs) for solar power applications. We report here the results of a computational study to identify the surface coverages and adsorption sites which provide the largest adsorption energies and/or highest NEA values in the Sc–C, Sc–O–C and Sc–N–C systems, to help guide future experiments.

## 2. Computational details

Plane-wave density-functional theory (DFT) calculations were performed using the Cambridge Serial Total Energy Package (CASTEP) code [38]. The exchange-correlation parameters used were the Perdew–Burke–Ernzerhof (PBE) functional in the generalised gradient approximation (GGA) [39]. The Broyden–Fletcher–Goldfarb–Shanno (BFGS) algorithm was employed as a minimisation method in geometry optimisation [40]. A plane-wave basis set with an energy cut-off value of 800 eV (see details in the [Supplementary Information, section 1](#)) and ultrasoft Vanderbilt-type pseudopotentials in reciprocal space were used for all calculations [41]. Density-of-states (DOS) calculations were carried out using the OptaDOS code including DOS spacing of 0.01 eV and adaptive smearing of 0.8 eV [42]. The Brillouin zone (BZ) was sampled via Monkhorst–Pack  $k$ -point grids [43]. For the electronic-structure calculations with energy-minimisation steps and DOS calculations, special grids of  $6 \times 6 \times 1$  and  $12 \times 12 \times 1$   $k$ -points, respectively, were found to be the most useful. The atomic charges and bond populations were calculated using the Hirshfeld [44] and Mulliken [45] population-analysis schemes within a projection of the plane-wave states on the localised basis. The self-consistent field (SCF) convergence tolerances of total energy, ionic force, displacement and stress component were set to  $2.0 \times 10^{-5}$  eV/atom, 0.05 eV/ $\text{\AA}$ ,  $1.0 \times 10^{-3}$   $\text{\AA}$  and 0.10 GPa, respectively.

A  $2 \times 2$  supercell with (100) surface orientation was simulated using a slab of 14 carbon layers. Additional H, O, N and Sc atoms were used for terminations on both sides of the slab. The diamond slabs were periodic in the  $x$  and  $y$  planes with approximately  $\sim 18$ – $20 \text{ \AA}$  of vacuum separation in the  $z$ -direction to avoid interaction between slabs. The specified number of layers and the vacuum thickness have been widely used in previous DFT calculations, providing well-converged values of the final energy [18,23,35,46].

The adsorption energy ( $E_{ads}$ ) per adsorbate atom is calculated from

$$E_{ads} = \frac{1}{n} (E_{total} - E_0 - nE_{atom}) \quad (1)$$

where  $n$  is the number of adsorbate atoms in the supercell,  $E_{total}$  is the total energy of the surface supercell including the diamond slab and adsorbates,  $E_0$  is the energy of the diamond slab before the adsorbate in question (Sc, O or N) is added, and  $E_{atom}$  is the energy of an isolated

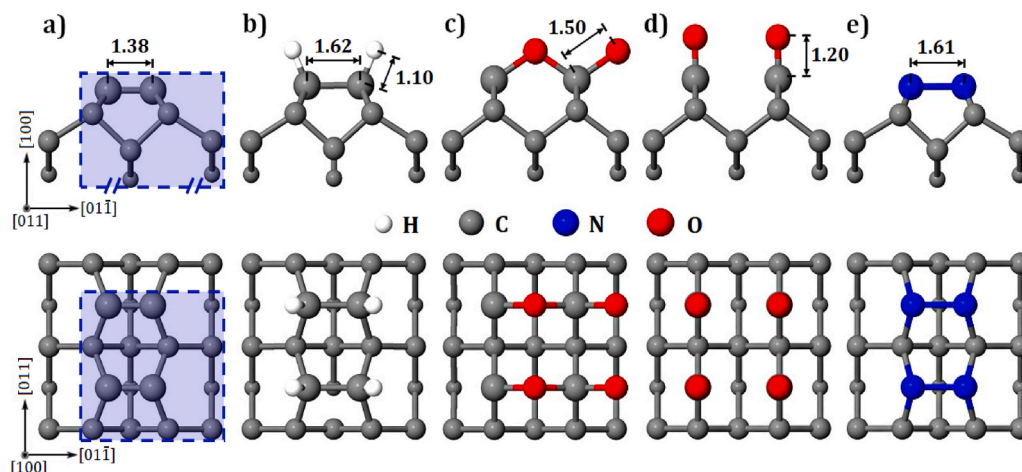


**Fig. 2.** Side and top views of the optimised geometries for (a) the bare ( $2 \times 1$ ), (b) hydrogenated ( $2 \times 1$ ), (c) oxygenated (ether) ( $1 \times 1$ ), (d) oxygenated (ketone, i.e. C=O double bond) ( $1 \times 1$ ), and (e) fully nitrogenated ( $2 \times 1$ ) diamond (100) surfaces. All lengths are in angstroms (Å). The blue dashed boxes indicate the ( $2 \times 2$ ) unit cell. White, grey, blue and red spheres are hydrogen, carbon, nitrogen and oxygen atoms, respectively.

adsorbate atom. For example, for the formation energy of the O-terminated surface,  $E_{\text{total}}$  is the energy of an O-terminated diamond slab,  $E_0$  is that of a bare diamond slab, and  $E_{\text{atom}}$  is the energy of the O atom. But for calculations of adsorption energies of Sc at the O-terminated surface,  $E_{\text{total}}$  is now the energy of the final ScO-terminated diamond slab,  $E_0$  is that for an oxygenated diamond slab, and  $E_{\text{atom}}$  is the energy of a Sc atom. Using Sc metal as the starting point for Sc incorporation rather than the Sc atom adds 3.918 eV per Sc atom to all the adsorption energies  $E_{\text{ads}}$  listed in the tables in this paper. All calculated adsorption energies in this work are exothermic.

The ionisation energy ( $I$ ) calculation for each surface is based on the energy difference between the vacuum and the valence-band maximum (VBM).

$$I = E_{\text{vac}} - E_{\text{VBM}} = (E_{\text{vac}} - V_{\text{av.slub}}) - (E_{\text{VBM, bulk}} - V_{\text{av. bulk}}) \quad (2)$$

$E_{\text{vac}}$  is the energy of the vacuum level which is set to zero,  $E_{\text{VBM}}$  is the energy of the VBM, while  $V_{\text{av.slub}}$  and  $V_{\text{av. bulk}}$  are the average electrostatic potential energies in the slab and bulk, respectively.  $E_{\text{VBM, bulk}}$  is

the VBM calculated for bulk diamond. The difference between  $E_{\text{VBM, bulk}}$  and  $V_{\text{av. bulk}}$  is equal to 10.52 eV which has already been computed [18]. The values for  $E_{\text{vac}}$  and  $V_{\text{av. bulk}}$  are extracted from the CASTEP binary check file using the *potId* CASTEP tool. This makes use of the macroscopic averages method of Fall et al. [47].

Due to the well-known underestimation of the band gap of diamond by GGA, the ‘scissor correction’ is applied [30]. Thus, the electron affinity (EA) value,  $\chi$ , is calculated from the ionisation energy by subtracting the experimental band gap ( $E_g = 5.47$  eV):

$$\chi = I - E_g \quad (3)$$

The work function ( $\varphi$ ) is defined as the minimum energy needed to move a surface electron to a point just outside the solid surface, and is calculated from

$$\varphi = E_{\text{vac}} - E_F \quad (4)$$

where  $E_F$  is the Fermi energy.

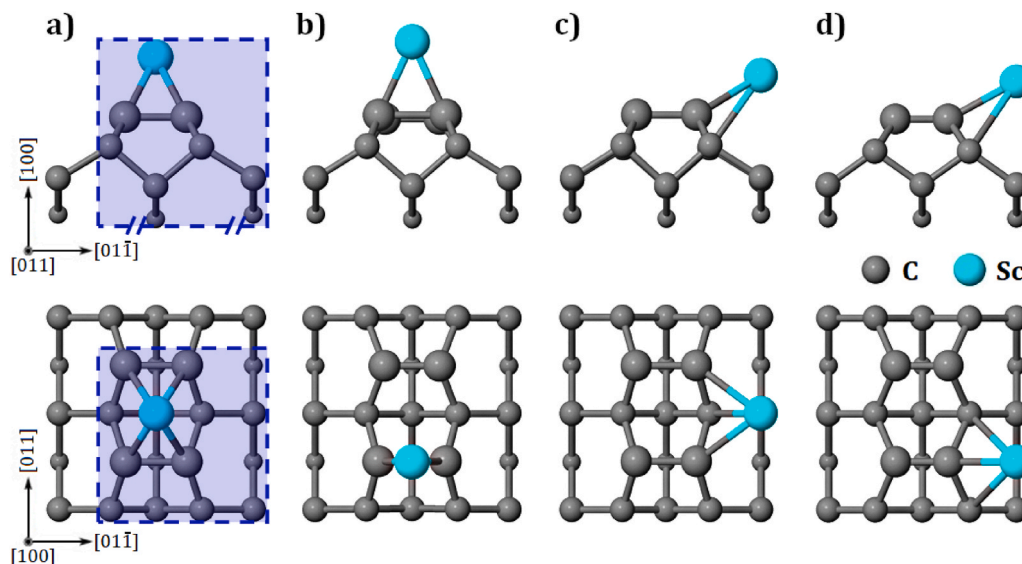


**Fig. 3.** Side and plan views of the ( $2 \times 1$ ) reconstructed diamond (100) surface with possible high-symmetry adsorption sites for 0.25 ML of Sc coverage: (a) pedestal (P), (b) bridge (B), (c) hollow (H), and (d) cave (C). The ( $2 \times 2$ ) unit cell is depicted as a blue box. Grey and cyan spheres correspond to C and Sc atoms, respectively.

**Table 1**

Calculated values of adsorption energy  $E_{\text{ads}}$ , ionisation energy  $I$ , electron affinity  $\chi$ , work function  $\phi$ , and respective bond lengths  $d$ , for the lowest-energy structures at 0.25 ML, 0.5 ML, and 1 ML surface coverages of Sc on the bare undoped diamond (100) surface. Geometry-optimisation calculations for the B and P + C positions at 0.5 and 1 ML, respectively, did not converge.

Coverage (ML)	Structure	$E_{\text{ads}}$ (eV/atom) <sup>c</sup>	$I$ (eV)	$\chi$ (eV)	$\phi$ (eV)	$d$ (C–C) (Å)	$d$ (C–Sc) (Å)
0.25	P	–5.37	2.45	–3.02	1.98	1.59	2.15
0.25	B	–4.45	3.99	–1.48	3.99	1.43, 1.75	2.07
0.25	H <sup>a</sup>	–5.92	2.71	–2.76	2.78	1.61	2.35
0.5	P (mirror)	–4.95	4.70	–0.77	3.85	1.71	2.24
0.5	H (mirror) <sup>b</sup>	–5.42	4.80	–0.67	3.72	1.68	2.38
0.5	P + H (zigzag) <sup>b</sup>	–6.17	5.18	–0.29	3.88	1.70	2.25, 2.41
0.5	P + H (linear)	–5.48	4.39	–1.08	3.37	1.61	2.31, 2.40
1	P + H	–4.39	5.81	0.34	3.48	1.65	2.43
1	B + H	–4.80	5.09	–0.38	3.39	1.64	2.43, 2.48
1	B + C	–4.25	4.39	–1.02	3.80	1.59	2.26, 2.44

<sup>a</sup> C sites at both 0.25 ML and 0.5 ML coverages were not added due to their relaxation to the H site.

<sup>b</sup> B + C (zigzag), B + C (linear), P + C, B + H positions at 0.5 ML were not included due to their instability. These geometries spontaneously relaxed to P + H (zigzag).

<sup>c</sup> Using Sc metal as the starting point for Sc incorporation rather than the Sc atom adds 3.918 eV per Sc atom to all the adsorption energies  $E_{\text{ads}}$ .

### 3. Results and discussion

#### 3.1. Base geometries

To obtain a clear idea of the accuracy and reliability of the calculations, computational studies were initially performed on the bare, hydrogenated, oxygenated (ether or ketone) and nitrogenated diamond (100) surfaces, and results compared with known literature values. Fig. 2 shows the associated optimised configurations for the bare and H, O and N terminated surfaces. The electronic and structural properties of the underlying structures are in good agreement with those from other calculations (see Table S1 in the Supplementary Information, section 2). These calibration results confirm that the modelling method and surface models reproduce, to a reasonable degree of accuracy, both the previously measured experimental and calculated values for all of the important parameters of the surfaces in question, including the EA,  $E_{\text{ads}}$ , and relevant surface atom-atom distances. This gives us confidence in extending these simulation procedures to study Sc adsorption onto these surfaces.

#### 3.2. Surface adsorption sites for Sc

The  $2 \times 2$  supercell with four Sc atoms is indicated as one-monolayer (1 ML) in this work. For this size of supercell, there are also possible sub-ML coverages including 0.25 ML and 0.5 ML where one or two adsorbate atoms, respectively, are added to each side-position of a diamond slab.

For the clean diamond surface, a  $(2 \times 1)$  surface reconstruction consisting of symmetric dimers has been obtained in GGA energy minimisation calculations [18,30,35,48]. Fig. 3 shows the most plausible adsorption sites previously suggested for alkali and TMs directly bonded to the  $(2 \times 1)$  diamond (100) surface, namely the pedestal (P), bridge (B), hollow (H) and cave (C) positions [19,23,49]. Only one of these possible sites is occupied by Sc at a coverage of 0.25 ML, while for increased coverages, such as 0.5 ML and 1 ML, a range of positions are occupied. For 0.5 ML coverage, high-symmetry sites, including ‘mirror’ and ‘linear’, and ‘zigzag’ (*i.e.*  $\sqrt{2} \times \sqrt{2}$ ) configurations are possible. When the adsorbate atoms of the Sc are situated vertically above the symmetric dimers, these configurations are termed ‘mirror’. In ‘linear’ configurations, Sc atoms lie on the dimer row for one half of the  $4 \times 2$  supercell whilst two Sc atoms are diagonally across the (100) surface lying on the dimer row and between them, in a ‘zigzag’ configuration (see Fig. S2). At 1 ML coverage, two ‘mirror’ configurations together form unique high-symmetry configurations.

##### 3.2.1. Sc on the bare (100) diamond surface

A summary of the calculated electronic and structural properties of Sc adsorbed on different sites on the bare diamond (100) surface is given in Table 1, while Fig. 4 shows the associated minimum-energy structures for various surface coverages. The H, P + H (zigzag) and B + H sites are found to be the minimum-energy configurations for 0.25, 0.5 and 1 ML coverages of Sc, respectively. Sc adsorbs strongly at these high-symmetry sites on the bare surface. When Sc is placed in other

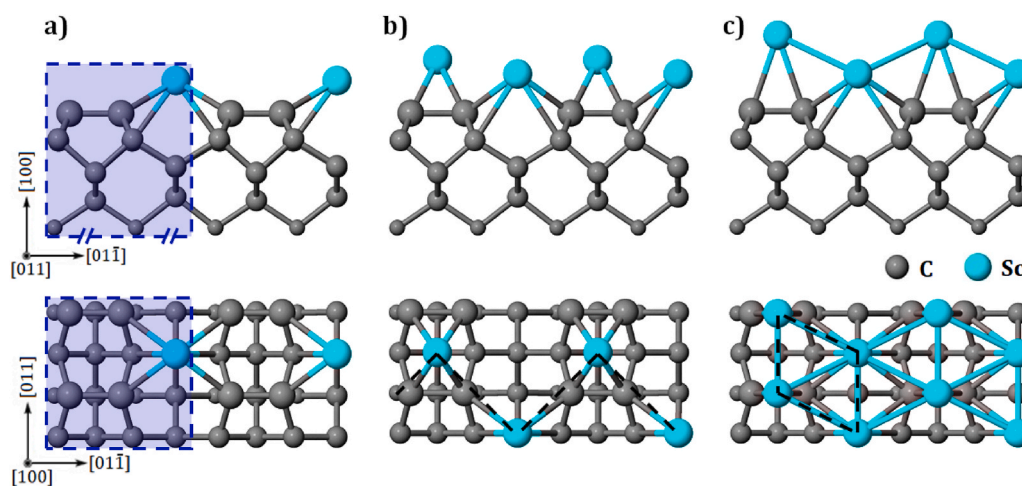


**Fig. 4.** Side and top views of the Sc-adsorbed bare diamond (100) surface of the lowest-energy optimised geometries of (a)–(c) 0.25, 0.5 and 1 ML, respectively. The  $(2 \times 2)$  unit cell is represented by a blue box for 0.25 ML whilst the dashed black lines indicate the zigzag and rhombus arrangements for 0.5 and 1 ML coverages of Sc, respectively, in the  $4 \times 2$  supercell. Grey and cyan spheres are C and Sc atoms, respectively.

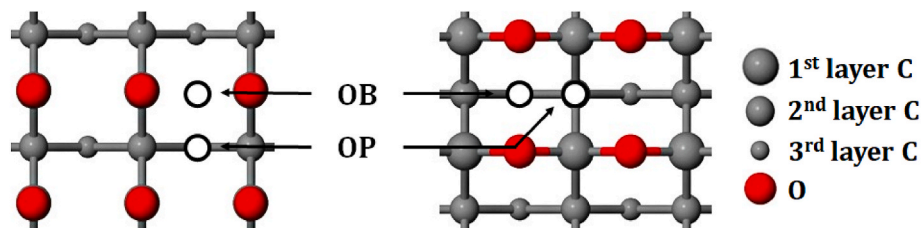


Fig. 5. Plan view depicting the two high-symmetry sites for adsorption on the O-terminated diamond (100) surface: OB = oxygen bridge and OP = oxygen pedestal positions. Grey and red spheres represent carbon and oxygen atoms, respectively.

potential adsorption sites at coverages of 0.25 and 0.5 ML, reconstruction to more favourable structures, H and P + H (zigzag), respectively, takes place. For 1 ML coverage, in the lowest-energy structures, the Sc atoms form parallelogram arrangements of Sc atoms: a square for the P + H and B + C sites, and a rhombus for B + H. These arrangements are similar to those reported previously for the Al-adsorbed (1 ML) bare diamond (100) surface described in Ref. [35].

The 0.5 ML Sc-adsorbed surface exhibits much more structural diversity than the 0.25 ML or 1 ML coverages, and there are P and H sites for mirror configurations, and P + H for both linear and zigzag configurations. These optimised geometries show stronger interactions between C and Sc atoms with shorter Sc–C bond lengths of 2.24–2.41 Å. Thus, the most energetically stable Sc-terminated (100) diamond surface is found to be P + H (zigzag) with a corresponding adsorption energy of –6.17 eV per Sc adsorbate for 0.5 ML coverage. Furthermore, the adsorption energies for Sc when forming the other two structures, H and P + H (linear) at 0.5 ML, are greater than the predicted adsorption energy of –5.27 eV when the H-terminated bare diamond (100) surface is formed (see Table S1). This suggests the Sc-adsorbed bare surface is more stable than hydrogenated diamond (100), and so should be practical for thermionic emission devices as a thermally stable surface.

Sc addition to the bare (2 × 1) reconstructed surface leads to the lengthening of the C–C dimer bond from 1.38 Å (see Fig. 2a)–1.43–1.75 Å, suggesting a change from a double bond to an elongated single-bond. This is seen in the accompanying decrease in the Mulliken bond population of the C–C dimer bond from 1.36 to 0.53–0.90 following Sc adsorption. Moreover, there is a correlation between the Mulliken populations of the Sc–C<sub>dimer</sub> bonds and the adsorption energies; larger adsorption energies are associated with a decrease of the Sc–C<sub>dimer</sub> bond populations. The values of the Sc–C<sub>dimer</sub> bond populations are 0.22, 0.12 and 0.06 for the most energetically favourable configurations at 0.25, 0.5 and 1 ML coverages, respectively.

We stress here that the magnitudes of the EA and work-function are extremely dependent upon the surface coverage and location of the Sc adsorbates. Most of the indicated structures have NEA (except the P + H site at 1 ML) and a low work function. The most negative NEA value of

–3.02 eV corresponds to the P site at 0.25 ML coverage of Sc. The EA values of Sc on (100) diamond compare very favourably with, and are generally more negative than, reported EA values for alkali metals [18, 19], TMs [23], and metalloids [50,51] with the exception of Ti (–3.64 eV) at 0.25 ML coverage. However, Ti adsorbed on diamond (100) at 0.5 ML and 1 ML was predicted to exhibit PEA and the adsorption energies of Ti are less exothermic than those of Sc by more than 1.0 eV per Ti atom [23]. Our results suggest that further computational studies of Sc at other terminations, such as oxygenated and nitrogenated diamond, are worthwhile. The highest adsorption energies and the most negative EA values for the Sc-adsorbed bare surface are summarised and discussed in section 3.2.3.

### 3.2.2. Sc on oxygenated (100) diamond

Sc adsorption on both the ether-like and ketone-like oxygenated diamond surfaces were also examined in this study. The number of high-symmetry adsorption sites on the oxygenated (1 × 1) surface decreases to two possible arrangements, similar to those for the bare surface (see Fig. 3) [18]. Thus, a pair of ‘mirror sites’ for the bare surface, including B and C, or P and H, are equivalent here since there are the same 2- and 4-coordinated sites. As shown in Fig. 5, these two sites are designated the oxygen-bridge (OB) position, where a single 2-coordinate Sc adsorbate surrounds the nearest two O positions, and the oxygen-pedestal (OP) position, where a 4-coordinate Sc has four O bonding neighbours.

In order to identify the lowest-energy arrangement, high-symmetry sites on the Sc-adsorbed (2 × 1) reconstructed O-terminated surface were also considered, despite the usual instability with respect to reconstruction of the bare (2 × 1) oxygenated surface. In this case, accommodation of the Sc adsorbate atoms stabilised the underlying O-layer, and the calculated electronic and structural properties are listed in Table 2.

The attachment of Sc to an oxygenated surface breaks one of the existing bonds, either a  $\pi$ -bond of the ketone (C=O) or a  $\sigma$ -bond of the ether (C–O–C). Most Sc adsorption occurs at ketone O-termination sites, which then relax to a (2 × 1) reconstruction. At 0.25 ML Sc coverage, Sc addition to the OP configuration occurs at the P and H sites. At 0.5 ML

Table 2

Calculated values of adsorption energy  $E_{\text{ads}}$ , ionisation energy  $I$ , electron affinity  $\chi$ , work function  $\phi$ , and respective bond lengths  $d$ , for the lowest-energy structures at 0.25 ML, 0.5 ML and 1 ML surface coverages of Sc onto an oxygenated undoped diamond (100) surface. OP (oxygen-pedestal) and OB (oxygen-bridge) indicate the individual (1 × 1) surface sites. E and K refer to the ether and ketone arrangements, respectively. Geometry optimisation of B at 0.5 ML and of P + C at 1 ML did not converge.

Coverage (ML)	Structure	$E_{\text{ads}}$ (eV/atom) <sup>c</sup>	$I$ (eV)	$\chi$ (eV)	$\phi$ (eV)	$d$ (C–C) (Å)	$d$ (C–O) (Å)	$d$ (O–Sc) (Å)
0.25	P (OP)–K	–7.81	1.74	–3.73	1.43	1.67	1.35	1.98
0.25	H <sup>†</sup> (OP)–K	–8.68	2.19	–3.28	1.86	1.63	1.34	1.94
0.5	P (mirror, OP)–E, K	–6.77	5.09	–0.38	3.60	1.67	1.39	2.05
0.5	H (mirror, OP)–K	–7.32	5.29	–0.18	3.69	1.63	1.38	2.02
0.5	P + H (zigzag, OP)–K	–8.25	5.91	0.44	3.85	1.65	1.39	2.02, 2.07
0.5	P + H (linear, OP)–K	–7.15	4.71	–0.76	3.27	1.63	1.39	1.97, 2.11
1	P + H (OP)–K	–5.09	6.35	0.88	3.97	1.63	1.39	2.11, 2.44
1	B + H (OP + OB)–K	–5.31	5.93	0.46	3.61	1.62	1.38	2.08, 2.27
1	B + C (OB)–K	–4.69	5.05	–0.42	4.06	1.63	1.38	1.98, 2.08

<sup>a</sup> C sites at both 0.25 ML and 0.5 ML coverages were not considered due to their relaxation to H.

<sup>b</sup> B + C (zigzag), B + C (linear), P + C and B + H positions at 0.5 ML are unstable, and these geometries spontaneously relaxed to the P + H (zigzag, OP) site.

<sup>c</sup> Using Sc metal as the starting point for Sc incorporation rather than the Sc atom adds 3.918 eV per Sc atom to all the adsorption energies  $E_{\text{ads}}$ .

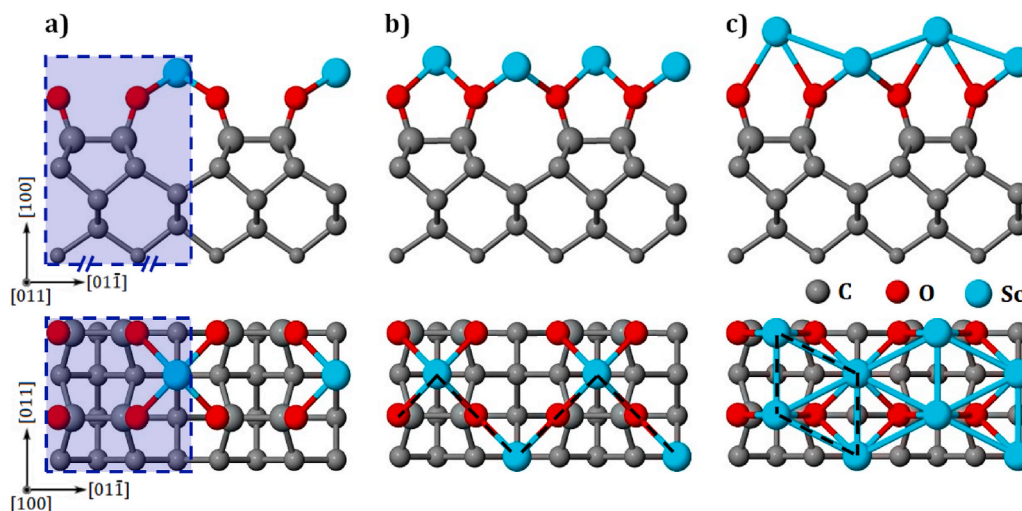


**Fig. 6.** Side and plan views of the minimum-energy optimised geometries for Sc coverages of (a) 0.25 ML, (b) 0.5 ML, and (c) 1 ML on an oxygenated diamond (100) surface. The  $(2 \times 2)$  unit cell is represented by a blue box for 0.25 ML whereas the dashed black lines indicate the zigzag and rhombus configurations for Sc coverages of 0.5 and 1 ML, respectively, in the  $4 \times 2$  supercell. Grey, red and cyan spheres are C, O and Sc atoms, respectively.

coverage, Sc also adsorbs at the OP positions but then relaxes into the P and H sites, which can exist separately as mirror configurations, or, alternatively, reconfigure to give P + H (linear) or (zigzag) structures as given in Table 2. For 1 ML coverage of Sc, two available adsorption configurations, OP and OB, are possible, which then convert to the P + H and B + C sites, respectively. However, a combination of an equal mixture of OP + OB (*i.e.* B + H) is the most stable. Here, the B + H site behaves as in the bare surface at the same coverage (see section 3.2.1), with the 4 Sc atoms forming a rhombus. For sub-ML coverages of 0.25 ML and 0.5 ML, the H and P + H (zigzag) sites are the minimum-energy positions, respectively, and the corresponding geometries are shown in Fig. 6.

CO bond lengths at the oxygenated (100) surface are 1.20 Å and 1.50 Å for ketone and ether linkages, respectively (see Fig. 2c, (d)). The calculated Mulliken bond populations for these bonds are 0.57 (ether) and 1.21 (ketone). With addition of Sc, the C=O ketone double-bond lengthens to 1.34–1.35 Å for 0.25 ML and to 1.38–1.39 Å at both 0.5 ML and 1 ML coverages (see Table 2). These bond lengths are slightly smaller than analogous values reported previously for Ti (0.25 ML, 1.36 Å; 0.5 ML, 1.38 Å; 1 ML, 1.39 Å) [29] and Al (0.25 ML, 1.36 Å; 0.5 ML, 1.34–1.41 Å; 1 ML, 1.39–1.41 Å) [35]. This trend is consistent with the Mulliken bond populations, which slightly decrease from 0.75 to 0.66 for the same increases in Sc coverage. At the same time, the Mulliken population of the new Sc–O bond increases from 0.16 to 0.35.

The strong C–O and O–Sc bonds lead to highly thermodynamically stable configurations with respect to scenarios at the Sc-terminated bare surface. Overall, the adsorption energies of Sc are in the range  $-8.68$  to  $-4.69$  eV/atom. At low Sc coverages, these values suggest high thermal stability of the ScO surface termination. Adsorption energies were calculated relative to the ether-like arrangement reported in the literature [30,35]. The most exothermic adsorption is at the H site for 0.25 ML Sc. As depicted in Fig. 6, Sc on an O-terminated surface prefers the 4-coordinated site, which is more energetically favourable than the 2-coordinated site.

Adsorption energies (see Table 2) become less exothermic with increasing Sc coverage. This trend is the opposite of that seen for the other metals previously examined [18,29,35]. If the adsorption energy decreases with coverage, then an island will have a higher energy (per Sc atom adsorbed) than an arrangement in which the Sc atoms are separated from each other. Thus, islands are thermodynamically unstable. Moreover, since the Sc–O bond energy is larger than the Sc–Sc bond energy, aggregation to form multi-layer clusters of Sc, either as 3D clusters or 2D islands, is thermodynamically unfavourable with respect

**Table 3**

Calculated most-negative electron affinities (EA) with corresponding adsorption energies ( $E_{\text{ads}}$ ) of different metal adsorbates on the oxygenated diamond (100) surface.

Termination	Coverage (ML)	EA (eV)	$E_{\text{ads}}$ (eV)	Type of calculation	Ref.
Li	1	-3.50	-3.64	DFT-GGA	[30]
Na	1	-1.42	-1.62	DFT-GGA	[30]
K	0.25	-2.44	-2.44	DFT-GGA	[30]
Cs	0.25	-2.41	-2.19	DFT-GGA	[30]
Mg	0.5	-3.28	-3.43	DFT-GGA	[30]
Ti	0.25	-3.10	-7.60	DFT-LDA <sup>a</sup>	[29]
Ni	0.5	-0.16	-3.80	DFT-LDA <sup>a</sup>	[29]
Cu	0.5	-1.28	-2.35	DFT-LDA <sup>a</sup>	[29]
Zn	0.5	-3.05	-1.13	DFT-LDA <sup>a</sup>	[29]
Al	1	-1.47	-4.11	DFT-GGA	[35]
Sc	0.25	-3.73	-7.81	DFT-GGA	present work

<sup>a</sup> LDA – the local density approximation of the exchange-correlation energy functional in DFT.

to isolated Sc atoms distributed uniformly over the diamond surface, making this system highly promising for large-scale manufacturing.

In contrast to Sc absorption onto a bare (100) diamond surface, adsorption on the oxygenated surface produces a mixture of PEA and NEA values at coverages of 0.5 ML and 1 ML. In comparison with previous theoretical studies of the diamond M–O–C system [18,29,30,35–37], ScO-termination has a larger NEA and a significantly more exothermic adsorption energy at all coverages. The largest NEA value of  $-3.73$  eV was observed for Sc in the P site at 0.25 ML, with a corresponding adsorption energy of  $-7.81$  eV per Sc atom. By way of comparison, calculated values for other metals at the O-terminated surface are summarised in Table 3. The largest NEA values and the highest adsorption energies for ScO-termination are discussed later in section 3.2.3.

### 3.2.3. Sc on nitrogenated (100) diamond

Compared with both M–C and M–O–C terminations, the M–N–C system is a relatively unexplored subject in the framework of EA studies on diamond. Nitrogen is trivalent, whereas each of the surface (100) C atoms can only form two bonds to an adsorbate, resulting in a dangling bond on the N atom which is energetically unfavourable. Thus, the surface reconstructs to form pairs of N–N dimer bonds, as shown in Fig. 2e.

**Table 4**

Calculated values of adsorption energy  $E_{\text{ads}}$ , ionisation energy  $I$ , electron affinity  $\chi$ , work function  $\phi$ , and respective bond lengths  $d$ , for the lowest-energy structures at 0.25, 0.5 and 1 ML surface coverages of Sc on a nitrogenated undoped diamond (100) surface. NP and NB indicate nitrogen-pedestal and nitrogen-bridge sites on the (1 × 1) unreconstructed surface. Geometry optimisation of C site at 0.25 ML, and P (mirror), B + C (linear) positions at 0.5 ML, did not converge.

Coverage (ML)	Structure	$E_{\text{ads}}$ (eV/atom) <sup>b</sup>	$I$ (eV)	$\chi$ (eV)	$\phi$ (eV)	$d$ (C–C) (Å)	$d$ (C–N) (Å)	$d$ (N–Sc) (Å)
0.25	P (NP)	–7.60	3.72	–1.75	2.29	1.57	2.48, 2.50	2.10
0.25	B (NB)	–6.10	4.08	–1.39	2.70	1.56	2.47, 2.49	1.93
0.25	H (NP)	–7.60	3.78	–1.69	2.34	1.57	2.48, 2.50	2.10
0.5	B, C (mirror, NB)	–5.03	4.69	–0.78	3.28	1.56	1.50, 2.49	2.08
0.5	H (mirror, NP)	–5.41	5.53	0.06	3.89	1.56	1.52, 2.48	2.17
0.5	P + H (zigzag, NP) <sup>a</sup>	–6.80	6.01	0.54	4.07	1.57	1.52, 2.51	2.17
0.5	B + C (zigzag, NB)	–6.02	5.26	–0.21	3.78	1.55	1.51, 2.49	2.03
0.5	P + H (linear, NP)	–5.85	5.45	–0.02	3.86	1.55	1.53, 2.49	2.16
1	P + H (NP)	–4.24	6.20	0.73	4.40	1.55	1.53, 2.53	2.28, 2.53
1	P + C, B + H (NB + NP)	–4.66	5.86	0.39	3.88	1.55	1.52, 2.49	2.21, 2.35
1	B + C (NB)	–4.47	5.77	0.30	4.22	1.55	1.51, 2.50	2.08, 2.32

<sup>a</sup> P + C and B + H positions at 0.5 ML are unstable, and both structures spontaneously relaxed to the P + H (zigzag, NP) site.

<sup>b</sup> Using Sc metal as the starting point for Sc incorporation rather than the Sc atom adds 3.918 eV per Sc atom to all the adsorption energies  $E_{\text{ads}}$ .

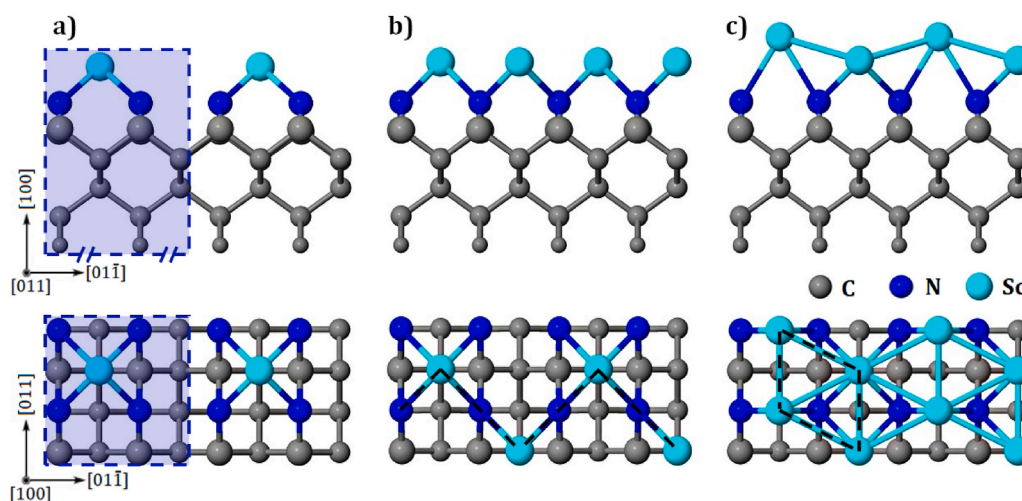


**Fig. 7.** Side and top views of the lowest energy optimised structures for Sc coverages of (a) 0.25 ML, (b) 0.5 ML, and (c) 1 ML for the Sc-terminated nitrogenated diamond (100) surface. The blue boxes indicate the (2 × 2) unit cell for 0.25 ML, while the dashed black lines represent a zigzag and rhombus configuration for 0.5 and 1 ML of Sc, respectively, in the 4 × 2 supercell. Grey, blue and cyan spheres are C, N and Sc atoms, respectively.

There are two possible Sc adsorption sites: the nitrogen bridge (NB) and nitrogen pedestal (NP) positions, resembling the OB and OP sites described in section 3.2.2. Due to the three-coordinate preference of nitrogen, an extensive array of optimised geometries is possible, in contrast to the relatively small number of geometries for the bare and oxygenated diamond surfaces. Computed electronic and structural properties of the available structures are given in Table 4, and the minimum-energy structures for the various coverages of the Sc-adsorbed N-terminated surface are depicted in Fig. 7.

Sc addition to a full-ML nitrogenated diamond (100) surface occurs in the same way as for the bare surface, by Sc adsorbing onto high-symmetry sites, which then rearrange to a lower energy configuration. In most scenarios, adsorption of Sc breaks both N–N dimer bonds, excluding the B and H arrangements where only the closest N–N bond to the Sc is broken. Breaking the N–N dimer bond causes the surface to revert to (1 × 1). The N–N dimer bond length in the nitrogenated surface with 1 ML of nitrogen is 1.61 Å (see Fig. 2e), with the Mulliken bond populations for N–N and C–N of 0.48 and 0.66, respectively. Following Sc adsorption, the C–N bond populations slightly increase to 0.71–0.78, in contrast to the corresponding decrease in the C–O bond population on Sc adsorption described in section 3.2.2. This is consistent with the decrease in the Mulliken populations of the Sc–N bonds, 0.32, 0.21 and 0.11 for the most energetically favourable configurations at 0.25, 0.5 and 1 ML Sc coverage, respectively.

As with ScO-terminated sites, the pedestal (NP) arrangement relaxes

into the 4-coordinated P and H positions for mirror, linear and zigzag configurations at all coverages. Moreover, the minimum-energy configurations are found to be both P and H at 0.25 ML, and P + H (zigzag) at 0.5 ML coverage of Sc. Conversely, the 2-coordinated bridge (NB) structures are the B and H sites for sub-ML and full-ML coverages. With 1 ML ScN-termination, rearrangement of the NP and NB sites provides the lowest-energy structures as the P + C and B + H positions have the same adsorption energy (–4.66 eV/atom). In both structures four Sc atoms form a rhombus configuration, as shown in Fig. 7c, similar to those at the Sc-terminated bare and oxidised surfaces.

ScN-terminated surfaces exhibit NEA and PEA at 0.25 and 1 ML coverages, respectively. The P and H sites at 0.25 ML were shown to have the largest magnitude NEA of –1.75 eV, and the highest adsorption energy of –7.60 eV per Sc atom. In contrast, the highest PEA configuration (0.74 eV) is P + H at 1 ML Sc.

Adsorption energies were calculated with respect to a (2 × 1) N-terminated structure (see Fig. 2e). For all the structures with 1 ML Sc coverage, the adsorption energies for Sc onto the nitrogenated diamond surface are lower than the calculated value of adsorption energy (–5.27 eV) for hydrogen onto a bare diamond (100) surface (see Table S1). As with ScO-terminations, increased surface coverage of Sc on N-terminated diamond also leads to the adsorption energies becoming less exothermic, suggesting that the Sc coverage, in principle, could be tuned experimentally to avoid island formation on the surface.

To compare Sc-terminated bare, oxygenated, and nitrogenated

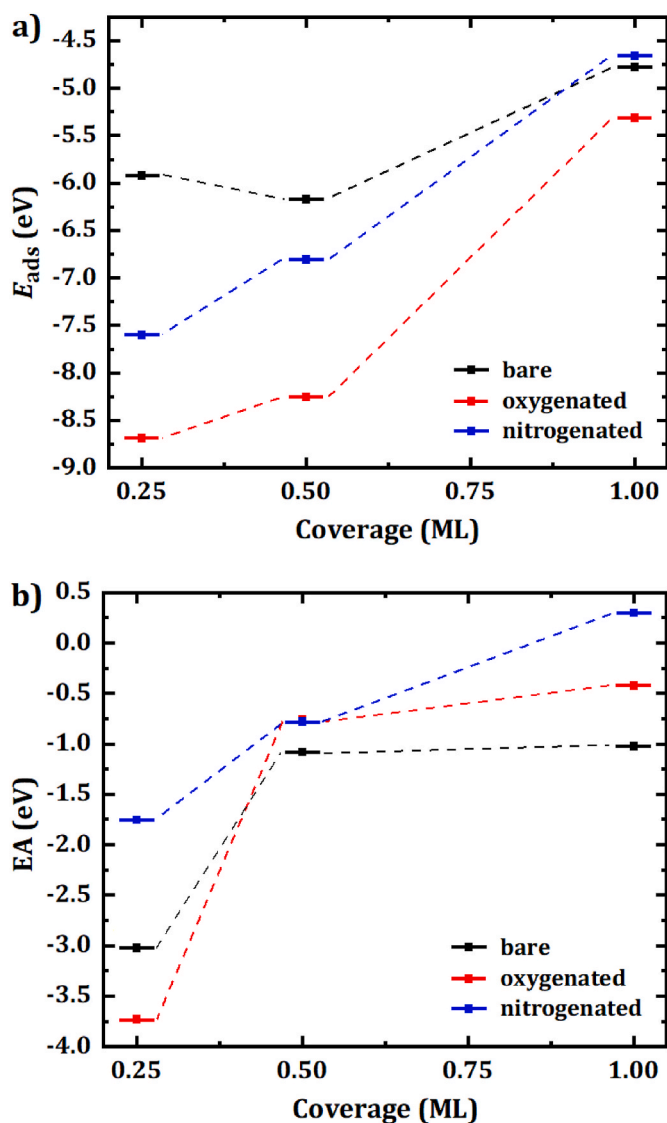


**Fig. 8.** A summary of the largest adsorption energies (a) and the most-negative EA values (b) at 0.25 ML, 0.5 ML, and 1 ML coverages for Sc-terminated bare, oxygenated, and nitrogenated diamond (100) surfaces. Values are taken from Tables 1, 2 and 4. The dashed lines indicate relevant coverages of Sc at each surface.

diamond (100) surfaces, the largest adsorption energies and the most negative EA values are collected together in Fig. 8 for different Sc coverages. Based upon Hirshfeld and Mulliken population analysis, Sc has a higher positive charge in the 4-coordinated sites (P and H) than when it is 2-coordinated (at B and C). Unlike Al [35], Sc favourably binds to the 4-coordinated sites at each surface, exhibiting larger adsorption energies and the most negative EA values.

As stated earlier in section 3.2.2, the strongest adsorption of Sc on diamond is found for the oxygenated surface at each coverage, indicating higher thermal stability at elevated temperatures. Adsorption energies at the different surface terminations follow the same trend as the tabulated bond enthalpies for Sc–C, Sc–O and Sc–N ( $444 \pm 21$  kJ mol<sup>-1</sup>,  $671.4 \pm 1.0$  kJ mol<sup>-1</sup> and  $464 \pm 84$  kJ mol<sup>-1</sup>, respectively [52]). As shown in Fig. 8a, increasing the Sc coverage on O-terminated diamond is accompanied by a decrease in adsorption energies, similar to that reported for Ti [29] and Al [35]. An identical trend is observed for adsorption to the N-terminated surface. In contrast, at 0.5 ML, Sc adsorbs strongly on the bare surface relative to 0.25 and 1 ML coverages.

The EA depends significantly on the location of the adsorbed Sc

atoms, as for previously studied metal adsorbates [18,23,29,30,35]. Increased surface coverage leads to less negative EA values at each surface, with a similar trend to that of the adsorption energies (Fig. 8b). The most negative EA values at 0.25 ML arise from the 4-coordinated sites (P) for all three differently terminated diamond surfaces, while the P + H (linear) site possesses the NEA at the 0.5 ML Sc-adsorbed bare and oxygenated diamond. In contrast, the NEA of 0.5 ML Sc on the N-terminated surface results from the 2-coordinated site (B + C). Furthermore, the EA magnitudes of the various Sc-terminated nitrogenated diamond surfaces are less negative than those of bare and oxygenated diamond, exhibiting positive EA values at full coverage. Thus, of the systems we have examined, we suggest both Sc-terminated bare and O-terminated diamond (100) surfaces are of great interest for subsequent experimental studies.

### 3.3. Electronic properties of Sc-adsorbed diamond (100)

We have examined in more detail the electronic properties of the selected Sc configurations with the highest adsorption energies and most negative EA values. The lowest Sc coverage (0.25 ML) was studied for three different surface terminations using projected density-of-states (PDOS) plots. The structures for these plots were taken from the lowest-energy configurations in Tables 1, 2 and 4, respectively. Detailed surface-charge-distribution plots were calculated for the most-negative EA configurations (see Supplementary Information, section 3).

We first investigated the PDOS plots of the bare, oxygenated (ether and ketone) and nitrogenated diamond (100) surfaces, to have a benchmark for these pristine surfaces. ‘Bulk’  $sp^3$  carbon atoms are those situated in the centre of the diamond slab, whilst ‘surface’  $sp^2$  carbons are in the dimer row (see Fig. S4). The presence of states lying within the band gap of bulk diamond can be seen in the plots, which are in excellent agreement with those from other DFT calculations [18,30,35,50,51].

The PDOS plots for the Sc-terminated bare, oxygenated (ketone) and nitrogenated surfaces at 0.25 ML coverage, are given in Fig. 9. We focus here on the ketone O-termination existing as a  $(2 \times 1)$  reconstructed surface because this has the largest associated Sc adsorption energy (see Table 2).

For Sc adsorbing on bare diamond, there are prominent bands, originating from the 3d and 4s states of Sc (Fig. 9a). The majority of these bands generally occur in the inter-bandgap region, overlapping with states from the surface C, leading to the Sc–C bonding discussed earlier. There are 3d and 4s states both below and above the Fermi level. At the ketone O-terminated surface, the Sc and O PDOS display a large number of peaks over a wide range of energies, including contributions from O 2p and Sc 3d and 4s within the band gap region. The 3d states are lower in energy here than in the PDOS of the bare surface, consistent with a higher charge on Sc; the Sc–O bond is more ionic than Sc–C. The PDOS plots for the Sc-terminated nitrogenated surface in Fig. 9c are intermediate between those for the bare and O-terminated surfaces, consistent with the relative electronegativities of C, O and N and the Mulliken charges on Sc. The 3d states here moved down in energy relative to the bare surface but not to the same extent as in Fig. 9b.

## 4. Conclusions

First-principles calculations were performed for Sc adsorption of up to 1 ML on clean, O- and N-terminated (100) diamond surfaces. Sc adsorbs most strongly on the O-terminated surface, with adsorption energies much larger than those on for the well-studied NEA surface of hydrogenated diamond, suggesting higher thermal stability ( $>1200$  °C) may be possible experimentally. Indeed, an extremely large adsorption energy of  $-8.68$  eV per adsorbate atom is predicted for 0.25 ML coverage of Sc on an O-terminated surface. These are much larger than those observed for any metal previously studied in the context (Table 3) [18,29,30,35]. Moreover, in contrast to other metal terminations, where only some of the possible adsorbate structures produced significant NEA

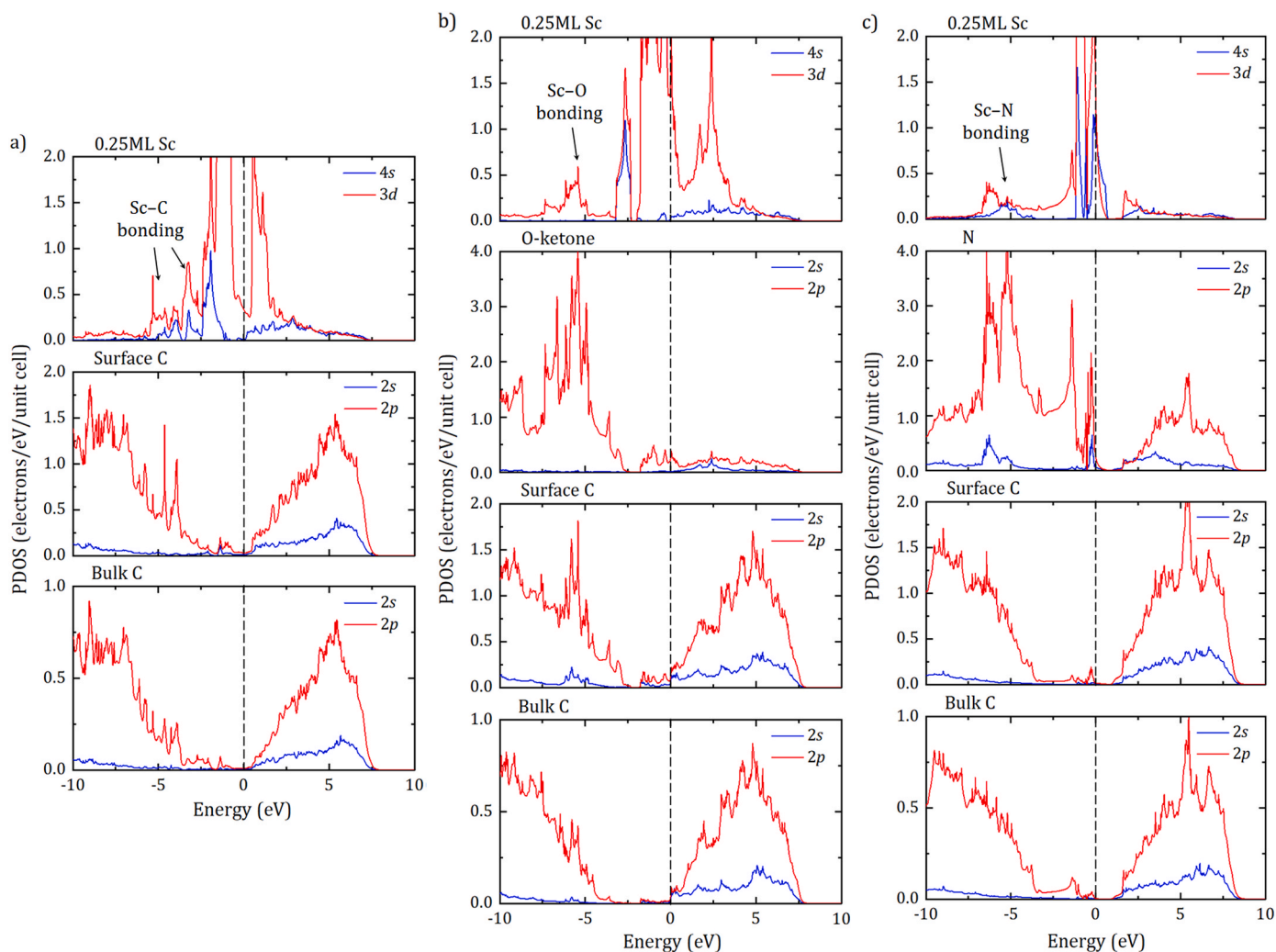


**Fig. 9.** PDOS for 0.25 ML Sc adsorption on the (a) bare, (b) oxygenated (ketone) and (c) nitrogenated diamond surfaces. These are the lowest-energy structures from Tables 1, 2 and 4, respectively. The dashed vertical lines correspond to the Fermi level which is arbitrarily set to zero. In each plot, the atom in question is labelled at the top right-hand side of each plot and its relevant orbitals are colour-coded. The top of the peaks of the 3d states are cut off.

and many have PEA, with scandium *most* of the Sc-adsorbed oxygenated, bare and nitrogenated diamond surfaces display substantial NEA; the most negative values are  $-3.73$  eV,  $-3.02$  eV and  $-1.75$  eV, respectively, for a Sc coverage of 0.25 ML. This suggests that experimentally, scandium termination may be more ‘forgiving’ of variations in deposition conditions than other M–O–C schemes, because whatever structure is produced will nevertheless result in NEA.

The predicted substantial NEA values for most likely adsorbate structures, extremely high adsorption energy (and therefore thermal stability), and the small thermodynamic likelihood of island formation, suggest that Sc–O–C and Sc–C terminated diamond surfaces may be the best candidate yet for electron-emission applications at elevated temperatures. As such, subsequent experimental work should focus on confirming these predictions for Sc adsorbed onto bare and O-terminated diamond surfaces, and measuring their NEA, surface stability and electron emission properties.

#### CRediT authorship contribution statement

**Ramiz Zulkharnay:** Methodology, Software, Formal analysis, Investigation, Writing – original draft. **Neil L. Allan:** Methodology, Validation, Writing – review & editing. **Paul W. May:** Methodology, Validation, Writing – review & editing, Supervision.

#### Declaration of competing interest

The authors declare that they have no known competing financial interests or personal relationships that could have appeared to influence the work reported in this paper.

#### Acknowledgements

RZ would like to acknowledge the funding scheme of the Government of the Republic of Kazakhstan under the Bolashak International programme. This work was carried out using the computational facilities of the Advanced Computing Research Centre, University of Bristol (<http://bris.ac.uk/acrc/>).

#### Appendix A. Supplementary data

Supplementary data to this article can be found online at <https://doi.org/10.1016/j.carbon.2022.04.067>. The raw data and computer input/output files for these calculations are available via the Bristol University data repository at <https://doi.org/10.5523/bris.36mect2yhyabk2j1amkvbwqlrw>.

## References

- [1] P.W. May, Diamond thin films: a 21st-century material, *Philos. Trans. R. Soc. A* 358 (2000) 473–495.
- [2] A. Mainwood, Recent developments of diamond detectors for particles and UV radiation, *Semicond. Sci. Technol.* 15 (2000) 55–63.
- [3] J. Hiscock, A.T. Collins, Comparison of diamond and silicon ultraviolet photodetectors, *Diam. Relat. Mater.* 8 (1999) 1753–1758.
- [4] A. Aleksov, M. Kubovic, N. Kaeb, U. Spitzberg, A. Bergmaier, G. Dollinger, Th. Bauer, M. Schreck, B. Stritzker, E. Kohn, Diamond field effect transistors—concepts and challenges, *Diam. Relat. Mater.* 12 (2003) 391–398.
- [5] H. Kawarada, H. Tsuboi, T. Naruo, T. Yamada, D. Yu, A. Daicho, T. Saito, A. Hiraiwa, C-H surface diamond field effect transistors for high temperature (400 °C) and high voltage (500 V) operation, *Appl. Phys. Lett.* 105 (2014), 013510.
- [6] Y. Sasama, T. Kageura, K. Komatsu, S. Moriyama, J. Inoue, M. Imura, K. Watanabe, T. Taniguchi, T. Uchihashi, Y. Takahide, Charge-carrier mobility in hydrogen-terminated diamond field-effect transistors, *J. Appl. Phys.* 127 (2020), 185707.
- [7] M. Kataoka, C. Zhu, F.A.M. Koeck, R.J. Nemanich, Thermionic electron emission from nitrogen-doped homoepitaxial diamond, *Diam. Relat. Mater.* 19 (2010) 110–113.
- [8] F.A.M. Koeck, R.J. Nemanich, A. Lazea, K. Haenen, Thermionic electron emission from low work-function phosphorus doped diamond films, *Diam. Relat. Mater.* 18 (2009) 789–791.
- [9] J. Hamers, J.A. Bandy, D. Zhu, L. Zhang, Photoemission from diamond films and substrates into water: dynamics of solvated electrons and implications for diamond photoelectrochemistry, *Faraday Discuss* 172 (2014) 397–411.
- [10] M.C. James, F. Fogarty, R. Zulkarnay, N.A. Fox, P.W. May, A review of surface functionalisation of diamond for thermionic emission applications, *Carbon* 171 (2021) 532–550.
- [11] C. Bandis, B.B. Pate, Electron emission due to exciton breakup from negative electron affinity diamond, *Phys. Rev. B* 52 (1995) 12056–12071.
- [12] K.P. Loh, J.S. Foord, R.G. Edgell, R.B. Jackman, Tuning the electron affinity of CVD diamond with adsorbed caesium and oxygen layers, *Diam. Relat. Mater.* 5 (1997) 874–878.
- [13] L. Diederich, O.M. Küttel, P. Aebi, L. Schlapbach, Electron affinity and work function of differently oriented and doped diamond surfaces determined by photoelectron spectroscopy, *Surf. Sci.* 418 (1998) 219–239.
- [14] J.B. Cui, J. Ristein, L. Ley, Electron affinity of the bare and hydrogen covered single crystal diamond (111) Surface, *Phys. Rev. Lett.* 81 (1998) 429–432.
- [15] F. Maier, J. Ristein, L. Ley, Electron affinity of plasma-hydrogenated and chemically oxidized diamond (100) surfaces, *Phys. Rev. B* 64 (2001), 165411.
- [16] D. Takeuchi, S.-G. Ri, H. Kato, C.E. Nebel, S. Yamasaki, Negative electron affinity on hydrogen terminated diamond, *Phys. Status Solidi* 11 (2005) 2098–2103.
- [17] W.F. Paxton, M. Howell, W.P. Kang, J.L. Davidson, Influence of hydrogen on the thermionic electron emission from nitrogen-incorporated polycrystalline diamond films, *J. Vac. Sci. Technol. B* 30 (2012) 21202.
- [18] K.M. O'Donnell, T.L. Martin, N.A. Fox, D. Cherns, *Ab initio* investigation of lithium on the diamond, C(100) surface, *Phys. Rev. B* 82 (2010), 115303.
- [19] J.L. Nie, H.Y. Xiao, X.T. Zu, First principles calculations on Na and K-adsorbed diamond (100) surface, *Chem. Phys.* 326 (2006) 308–314.
- [20] J. Van Der Weide, R.J. Nemanich, Schottky barrier height and negative electron affinity of titanium on (111) diamond, *J. Vac. Sci. Technol. B* 10 (1992) 1940–1943.
- [21] P.K. Baumann, R.J. Nemanich, Characterization of copper-diamond (100), (111), and (110) interfaces: electron affinity and Schottky barrier, *Phys. Rev. B* 58 (1998) 1643–1654.
- [22] P.K. Baumann, R.J. Nemanich, Electron affinity and Schottky barrier height of metal–diamond (100), (111), and (110) interfaces, *J. Appl. Phys.* 83 (1998) 2072–2082.
- [23] A.K. Tiwari, J. Goss, P.R. Briddon, N.G. Wright, A.B. Horsfall, M.J. Rayson, Electronic and structural properties of diamond (001) surfaces terminated by selected transition metals, *Phys. Rev. B* 86 (2012), 155301.
- [24] K.M. O'Donnell, M.T. Edmonds, J. Ristein, A. Tadich, L. Thomsen, Q.-H. Wu, C. I. Pakes, L. Ley, Diamond surfaces with air-stable negative electron affinity and giant electron yield enhancement, *Adv. Funct. Mater.* 23 (2013) 5608–5614.
- [25] K.M. O'Donnell, M.T. Edmonds, A. Tadich, L. Thomsen, A. Stacey, A. Schenk, C. I. Pakes, L. Ley, Extremely high negative electron affinity of diamond via magnesium adsorption, *Phys. Rev. B* 92 (2015), 035303.
- [26] K. Larsson, The combined influence of dopant species and surface termination on the electronic properties of diamond surfaces, *J. Carbon Res.* 6 (2020) 22.
- [27] R. Yoshida, D. Miyata, T. Makino, S. Yamasaki, T. Matsumoto, T. Inokuma, N. Tokuda, Formation of atomically flat hydroxyl-terminated diamond (111) surfaces via water vapor annealing, *Appl. Surf. Sci.* 458 (2018) 222–225.
- [28] W. Shen, S. Shen, S. Liu, H. Li, Z. Gan, Q. Zhang, Monolayer cubic boron nitride terminated diamond (111) surfaces for quantum sensing and electron emission applications, *ACS Appl. Mater. Interfaces* 12 (2020) 33336–33345.
- [29] A.K. Tiwari, J. Goss, P.R. Briddon, A.B. Horsfall, N.G. Wright, R. Jones, M. J. Rayson, Unexpected change in the electron affinity of diamond caused by the ultra-thin transition metal oxide films, *Europhys. Lett.* 108 (2014) 46005.
- [30] K.M. O'Donnell, T.L. Martin, N.L. Allan, Light metals on oxygen-terminated diamond (100): structure and electronic properties, *Chem. Mater.* 27 (2015) 1306–1315.
- [31] M.C. James, M. Cattelan, N.A. Fox, R.F. Silva, R.M. Silva, P.W. May, Experimental studies of electron affinity and work function from aluminium on oxidised diamond (100) and (111) surfaces, *Phys. Status Solidi B* 258 (2021), 2100027.
- [32] W.E. Pickett, Negative electron affinity and low work function surface: caesium on oxygenated diamond (100), *Phys. Rev. Lett.* 73 (1994) 1664–1667.
- [33] K.M. O'Donnell, T.L. Martin, M.T. Edmonds, A. Tadich, L. Thomsen, J. Ristein, C. I. Pakes, N.A. Fox, L. Ley, Photoelectron emission from lithiated diamond, *Phys. Status Solidi* 211 (2014) 2209–2222.
- [34] S. Ullah, G. Wan, C. Kouzios, C. Woodgate, M. Cattelan, N.A. Fox, Structure and electronic properties of Tin monoxide (SnO) and lithiated SnO terminated diamond (100) and its comparison with lithium oxide terminated diamond, *Appl. Surf. Sci.* 559 (2021), 149962.
- [35] M.C. James, A. Croot, P.W. May, N.L. Allan, Negative electron affinity from aluminium on the diamond (100) surface: a theoretical study, *J. Phys. Condens. Matter* 30 (2018), 235002.
- [36] M.C. James, P.W. May, N.L. Allan, *Ab initio* study of negative electron affinity from light metals on the oxygen-terminated diamond (111) surface, *J. Phys. Condens. Matter* 31 (2019), 295002.
- [37] F. Fogarty, *Renewable Energy – Low Temperature Thermionic Emission from Modified Diamond Surfaces*, PhD Thesis, University of Bristol, UK, 2020, [http://www.chm.bris.ac.uk/pt/diamond/fabianthesis/Fabian\\_Fogarty\\_PhD\\_Thesis.pdf](http://www.chm.bris.ac.uk/pt/diamond/fabianthesis/Fabian_Fogarty_PhD_Thesis.pdf).
- [38] S.J. Clark, M.D. Segall, C.J. Pickard, P.J. Hasnip, M.L.J. Probert, K. Refson, M. C. Payne, First principles methods using CASTEP, *Z. Kristallogr.* 220 (2005) 567–570.
- [39] J.P. Perdew, K. Burke, M. Ernzerhof, Generalized gradient approximation made simple, *Phys. Rev. Lett.* 77 (1996) 3865–3868.
- [40] M.S. Bazaraa, H.D. Sherali, C.M. Shetty, *Nonlinear Programming, Theory and Algorithms*, second ed., John Wiley & Sons, Inc., New York, 1993.
- [41] D. Vanderbilt, Soft self-consistent pseudopotentials in a generalized eigenvalue formalism, *Phys. Rev. B* 41 (1990) 7892–7895.
- [42] A.J. Morris, R.J. Nicholls, C.J. Pickard, J.R. Yates, OptaDOS: a tool for obtaining density of states, core-level and optical spectra from electronic structure codes, *Comput. Phys. Commun.* 185 (2014) 1477–1485.
- [43] H.J. Monkhorst, J.D. Pack, Special points for Brillouin-zone integrations, *Phys. Rev. B* 13 (1976), 518892.
- [44] F.L. Hirshfeld, Bonded-atom fragments for describing molecular charge densities, *Theor. Chim. Acta* 44 (1977) 129–138.
- [45] R.S. Mulliken, Electronic population analysis on LCAO–MO molecular wave functions, *J. Chem. Phys.* 23 (1955) 1833–1840.
- [46] S.J. Sque, R. Jones, P.R. Briddon, Structure, electronics, and interaction of hydrogen and oxygen on diamond surfaces, *Phys. Rev. B* 73 (2006), 085315.
- [47] C.J. Fall, N. Binggeli, A. Baldereschi, Deriving accurate work functions from thin-slab calculations, *J. Phys. Condens. Matter* 11 (1999) 2689–2696.
- [48] B. Hammer, L.B. Hansen, J.K. Nørskov, Improved adsorption energetics within density-functional theory using revised Perdew-Burke-Ernzerhof functionals, *Phys. Rev. B* 59 (1999) 7413–7421.
- [49] Y. Jia, W. Zhu, E.G. Wang, Y. Huo, Z. Zhang, Initial stages of Ti growth on diamond (100) surfaces: from single adatom diffusion to quantum wire formation, *Phys. Rev. Lett.* 94 (2005), 086101.
- [50] W. Shen, Y. Pan, S. Shen, H. Li, Y. Zhang, G. Zhang, Electron affinity of boron-terminated diamond (001) surfaces: a density functional theory study, *J. Mater. Chem. C* 7 (2019) 9756–9765.
- [51] Z. Sun, M. Yang, X. Wang, P. Wang, C. Zhang, N. Gao, H. Li, Boron-terminated diamond (100) surfaces with promising structural and electronic properties, *Phys. Chem. Chem. Phys.* 22 (2020) 8060–8066.
- [52] Y.R. Luo, *Comprehensive Handbook of Chemical Bond Energies*, CRC Press, Boca Raton, FL, 2007.